DOI: 10.1002/asia.200800468

Syntheses, Photophysics, and Application of Iridium(III) Phosphorescent Emitters for Highly Efficient, Long-Life Organic Light-Emitting Diodes

Tsang-Chi Lee,[a] Chiung-Fang Chang,[a] Yuan-Chieh Chiu,[a] Yun Chi,*[a] Tzu-Ying Chan,[b] Yi-Ming Cheng,[b] Chin-Hung Lai,[b] Pi-Tai Chou,*[b] Gene-Hsiang Lee,[b] Chen-Han Chien,[c] Ching-Fong Shu,*[c] and Jens Leonhardt[d]

Abstract: Rational design and synthesis of Ir^{III} complexes (**1**–**3**) bearing two cyclometalated ligands (C^N) and one 2-(diphenylphosphino)phenolate chelate (P^O) as well as the corresponding Ir^{III} derivatives (**4**–**6**) with only one (C^N) ligand and two P^O chelates are reported, where (C^NH) = phenylpyridine (ppyH), 1-phenylisoquinoline (piqH), and 4-phenylquinazoline (nazoH). Single crystal X-ray diffraction studies of **3** reveal a distorted octahedral coordination geometry, in which two nazo ligands adopt an eclipsed configuration, with the third P^O ligand located *trans* to the phenyl group of both nazo ligands, confirming the general skeletal pattern for **1**–**3**. In sharp contrast, complex **4** reveals a *trans*-disposition for the PPh_2 groups, along with the phenolate groups residing opposite the unique cyclometalated ppy ligand, which is the representative structure for **4**–**6**. These Ir^{III} complexes exhibit green-to-red photoluminescence with moderate to high quantum efficiencies in the degassed fluid state and bright emission in the solid state. For **1**–**6**, the resolved emission spectroscopy and relaxation dynamics are well rationalized by the computational approach. OLEDs fabricated using 12 wt.% of **3** doped in CBP and with BCP as hole blocking material, give bright electroluminescence with $\lambda_{max} =$ 628 nm and CIE_{xy} coordinates (0.65, 0.34). The turn-on voltage is 3.2 V, while the current efficiency and the power efficiency reach 11.2 cd A^{-1} and 4.5 lm W^{-1} at 20 mA cm^{-2}. The maximum efficiency reaches 14.7 cd $A^{-1}$and 6.8 lm W^{-1} upon switching to TPBI as hole blocking material. For evaluating device lifespan, the tested device incorporating CuPc as a passivation layer, **3** doped in CTP as an emitting layer, and BAlq as hole blocking material, shows a remarkably long lifetime up to 36000 h at an initial luminance of 500 cd m^{-2}.

Keywords: density functional calculations · iridium · luminescence · OLEDs · photophysics

[a] T.-C. Lee, C.-F. Chang, Y.-C. Chiu, Prof. Y. Chi
Department of Chemistry
National Tsing Hua University
Hsinchu 300 (Taiwan)
Fax: (+886) 3-572-0864
E-mail: ychi@mx.nthu.edu.tw

[b] T.-Y. Chan, Dr. Y.-M. Cheng, C.-H. Lai, Prof. P.-T. Chou, Dr. G.-H. Lee
Department of Chemistry
National Taiwan University
Taipei 106 (Taiwan)
Fax: (+886) 2-2369-5208
E-mail: chop@ntu.edu.tw

[c] C.-H. Chien, Prof. C.-F. Shu
Department of Applied Chemistry
National Chiao Tung University
Hsinchu 30010 (Taiwan)
E-mail: shu@cc.nctu.edu.tw

[d] J. Leonhardt
Sensient Imaging Technologies GmbH
ChemiePark Bitterfeld-Wolfen, Areal A
Sensientstraße 3, 06766 Bitterfeld-Wolfen (Germany)

Introduction

Organometallic complexes possessing a third-row transition-metal element are crucial for the fabrication of highly efficient organic light-emitting diodes (OLEDs).[1] The strong spin-orbit coupling induced by a heavy metal ion such as iridium(III) promotes efficient intersystem crossing from the singlet to the triplet excited state manifold, which then facilitates strong electroluminescence by the harnessing of both singlet and triplet excitons induced by charge recombination. An internal phosphorescence quantum efficiency (η_{int}) of ~100% could be achieved, hence, these heavy metal containing emitters would be superior to their fluorescent counterparts in the fabrication of OLEDs. As a result, there has been a continuous trend of shifting research endeavors to these heavy transition-metal based complexes.

In fact, the tri-substituted (or homoleptic) Ir^{III} complexes with formula $[Ir(C^N)_3]$, (C^N)H = 2-(4′,6′-difluorophenyl)

pyridine,[2] 2-phenyl pyridine,[3] and 1-phenyl isoquinoline,[4] have shown the anticipated blue, green, and red phosphorescence in both fluid and solid states and hence are highly desirable for the fabrication of phosphorescent OLEDs. Unfortunately, many cyclometalating ligands (C^N)H do not react with Ir^{III} reagents to give the designated homoleptic Ir^{III} complexes $[Ir(C^N)_3]$. Alternatively, researchers have turned to develop a distinctive class of heteroleptic complexes with formula $[Ir(C^N)_2(L^X)]$, L^X = ancillary anionic chelate, for which much higher product yields have been achieved.[5]

As for the photophysical properties, it has been reported that a wide range of anionic ancillary L^X ligands can be incorporated into these complexes $[(C^N)_2Ir(L^X)]$, in which L^X = acetylacetonate (acac),[6] *N*-methylsalicyliminate (sal),[7] picolinate (pic) and analogues,[8] carbamate,[9] and even 2-pyridyl azolate (pyaz) ligands. Note the azolates can be pyrazolate, triazolate, or tetrazolate.[10] These heteroleptic complexes retain the main characteristics of the parent fragment $[Ir(C^N)_2]$ to a large degree. A small change in the emission peak wavelength was noted, which varied according to the intrinsic nature of the ancillary L^X ligand. For instance, the observed red shift of emission λ_{max} is in the order of pic < sal ~ acac, which is proportional to their relative electron donor strengths, resulting in a reduction of the energy gap.[11]

As for the 2-pyridyl azolate (pyaz) class of L^X ligands, a similar dependence on the azolate fragments and the properties of the substituents on the azolates is also noted.[5b,12] We can thus select the pyaz ligands, ranging from the CF_3 substituted pyrazole (fppzH) and triazole (fptzH) or the more electron rich *tert*-butyl substituted pyrazole (bppzH), in an attempt to conduct subtle color tuning. The donor strengths of pyaz ligands are expected to follow the trend fptz < fppz < bppz, therefore, it is not surprising that the fptz substituted complex displays the most blue-shifted emission signal, while the bppz substituted complexes show relatively red-shifted emission from the Ir^{III} complexes possessing the same class of cyclometalated C^N ligands.

Despite the above superiority in color tuning, unfortunately, most of the L^X ligands, such as the acac ligand, are weak-field ligands. As a result, the chemical stabilities of the resulting complexes, as well as the relative energy gap for the metal centered *dd* transition, could not be as large as those incorporating strong-field ligands. This case is particularly true for the red-orange emitting complex $[(pq)_2Ir(acac)]$, pqH = phenylquinoline, for which an inferior device lifetime arising from the influence of protons from PEDOT:PSS has been reported,[13] making such a series of acac substituted materials less desirable for industrial OLED application.

In this paper, we report a systematic design, synthesis, and characterization of heteroleptic iridium(III) complexes possessing a functionalized 2-(diphenylphosphino)phenolate (P^O) chelate. We believe that this new class of P^O ligand, owing to the synergy of the π-accepting diphenylphosphino unit and electron donating phenolate fragment,[14] should act significantly different to the previously discussed ancillary ligands, such that this dual accepting/donating character is expected to exhibit certain unusual characteristics, such as better thermal stabilities, higher emission efficiencies, and enhanced intramolecular ππ stacking. Details are elaborated in the following sections.

Results and Discussion

Synthesis and Characterization

The chloride bridged dimers $[(C^N)_2Ir(\mu\text{-}Cl)]_2$, where (C^N)H stands for 2-phenylpyridine (ppyH), 1-phenylisoquinoline (piqH), or 4-phenylquinazoline (nazoH), were synthesized from the direct reaction employing $IrCl_3$·hydrate mixed with two equiv of (C^N)H ligand in refluxing methoxyethanol. Subsequent treatment of $[(C^N)_2Ir(\mu\text{-}Cl)]_2$ with a stoichiometric amount of P^OH ligand in the presence of excess of Na_2CO_3 as proton scavenger gave isolation of the heteroleptic Ir^{III} complexes $[(C^N)_2Ir(P^O)]$ (**1**–**3**). On the other hand, according to the synthetic strategy that produced the mono-cyclometalated Ir^{III} complexes $[(C^N)Ir(L^X)_2]$,[15] treatment of $IrCl_3$·hydrate with a stoichiometric amount of (C^N)H ligand, followed by addition of two equiv of P^OH afforded the anticipated Ir^{III} complexes bearing two P^O ligands $[(C^N)Ir(P^O)_2]$ (**4**–**6**) in moderate to low yields. Their chemical structures are depicted in Scheme 1.

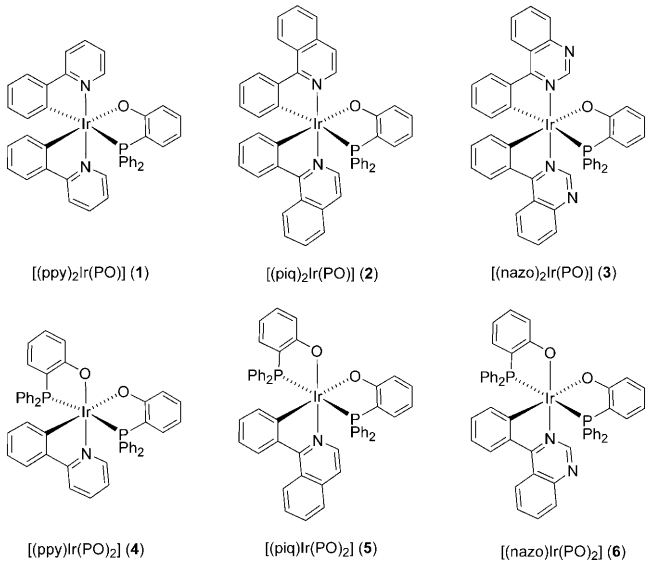

Scheme 1. Structural drawing of Ir^{III} complexes **1**–**6**.

The basic photophysical properties of $[(C^N)_2Ir(P^O)]$ complexes are, to a certain extent, analogous to the Ir^{III} complexes that possess similar cyclometalated ligands, despite them possessing distinctive ancillary ligands. Interestingly, introduction of two P^O ligands resulted in a significant variation of emission characteristics, as shown by the

photophysical data of $[(C^N)_2Ir(P^O)]$ (**1–3**) versus those of the $[(C^N)Ir(P^O)_2]$ counterparts (**4–6**). These differences will be elaborated in the section dealing with the photophysical data. In addition, all P^O chelated complexes **1–6** are highly soluble in chlorinated solvents and show negligible decomposition upon a raise in temperature. Detailed characterizations were conducted using MS, NMR, and elemental analysis (see Experimental Section), while complex **3** and **4** were further identified using single crystal X-ray analysis to establish their solid-state structure.

From the X-ray structural determination, complex **3** possesses a typical heteroleptic arrangement with two cyclometalating nazo chelates and one PPh_2 substituted phenolate ligand (Figure 1). The nazo chelates adopt a mutually eclipsed configuration with their coordinated nitrogen atoms N(1) and N(3) and carbon atoms C(1) and C(15), being located in *trans*- and *cis*-orientation, respectively. Moreover, the third P^O chelate resides opposite to the carbon atoms of both nazo ligands. The overall ligand arrangement is akin to those of the chloride-bridged dimer $[(ppy)_2Ir(\mu\text{-}Cl)]_2$, as well as other heteroleptic complexes such as $[(dpqx)_2Ir(fppz)]$,[16] suggesting that the P^O chelate in our case is coordinated to the Ir^{III} center by a stereoselective replacement of chloride ligands in its precursor $[(nazo)_2Ir(\mu\text{-}Cl)]_2$. Moreover, the elongated Ir–C(1) distance (2.034(3) Å) versus the Ir–C(15) bond (1.984(3) Å) shows the notable *trans*-effect imposed by the PPh_2 fragment, while twisting of nazo ligands is caused by the repulsion between the pair of hydrogen atoms located on carbon atoms C(5), C(9) and C(19), C(23), respectively. Formation of such twisted cyclometalated ligands has been well established for complexes with either piq or nazo chelates in recent literature.[17]

Moreover, detailed analysis of the structural data revealed the presence of two sets of ππ stacking interactions (Figure 1b). The first one is ascribed to the ππ stacking between one phenyl group of the Ph_2P segment and the adjacent nazo chelate, for which the centroid–centroid contact is calculated to be 3.942 Å. The second nazo ligand is parallel to the nazo chelate of the adjacent molecule where an even stronger ππ stacking was observed with the centroid–centroid contact being reduced to 3.698 Å. In sharp contrast to the aforementioned case, we expected this intramolecular PPh_2-nazo ππ stacking interaction, observed in a crystal lattice, would be easily disrupted upon dissolution in organic solvents.

Figure 2 showed the crystal structure of **4**, for which its structural motif exhibits only one cyclometalated ppy and two phenolate chelates bearing PPh_2 substitution. It is notable that oxygen atoms O(1) and O(2) occupied a *cis*-disposition, while the phosphorus atoms P(1) and P(2) adopted a *trans*-disposition, which is consistent with the large $J_{P,P}$ coupling constant (359 Hz) observed in the ^{31}P NMR spectrum. A similar *trans* arrangement of phosphine ligands has been observed in the related Ir^{III} complexes such as *trans*-$[Ir(ppy)_2(PPh_3)_2]^+$ and $[Ir(ppy)(PPh_3)_2(H)L]^{0,+}$, L = MeCN, CO, CN^-;[18] all of which showed emission in the sky-blue to blue region partially owing to the stronger electron accepting character of phosphine that stabilize the metal d_π orbitals (vide infra). Moreover, the Ir–O(1) distance (2.086(3) Å) is shorter than the Ir–O(2) bond (2.140(3) Å). This result is again attributed to the weakened *trans*-effect exerted by the nitrogen donor versus the carbon donor atom. Notably, these Ir–O distances, as well as the Ir–P distances in **4**, are both shorter than the respective Ir–O and Ir–P distances observed in **3**. This discrepancy may be ascribed to the depletion of electron density at the central Ir^{III} cation by double phosphine coordination, resulting in the enhancement of the metal–ligand bond strength in **4**. Finally,

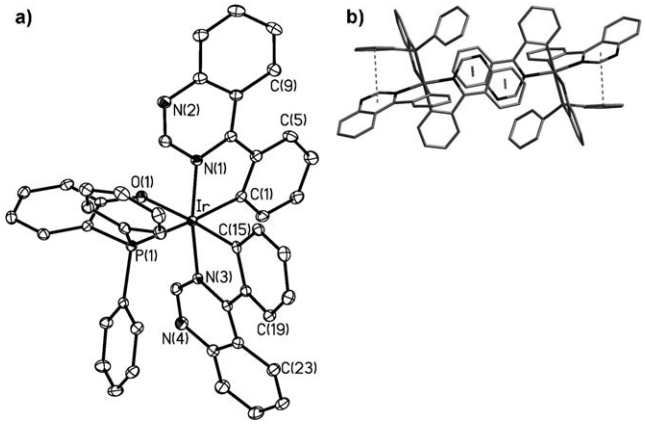

Figure 1. a) ORTEP diagram of **3** with thermal ellipsoids shown at 30% probability level; selected bond lengths (Å): Ir-C(1) = 2.034(3), Ir-C(15) = 1.984(3), Ir-N(1) = 2.057(3), Ir-N(3) = 2.030(3), Ir-P(1) = 2.3540(8), Ir-O(1) = 2.159(2) and selected bond angles (°): C(15)-Ir-N(3) = 79.43(12), C(1)-Ir-N(1) = 78.21(11), O(1)-Ir-P(1) = 81.60(6). b) Stacking diagram showing the centroid–centroid contacts between nazo ligands (dash, 3.698 Å) and between the dpp ligand and nazo chelate (dot line, 3.942 Å).

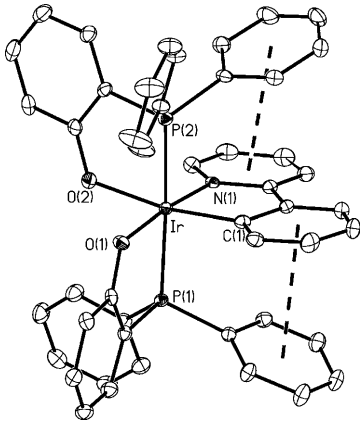

Figure 2. ORTEP diagram of **4** with thermal ellipsoids shown at 30% probability level; selected bond lengths (Å): Ir-C(1) = 2.016(3), Ir-N(1) = 2.021(3), Ir-O(1) = 2.086(3), Ir-O(2) = 2.140(3), Ir-P(1) = 2.3208(9), Ir-P(2) = 2.316(1) and selected bond angles (°): C(1)-Ir-N(1) = 80.68(14), O(1)-Ir-P(1) = 82.59(7), O(2)-Ir-P(2) = 82.49(7), P(1)-Ir-P(2) = 176.02(4). The centroid–centroid contacts from dpp ligand to the pyridyl and phenyl group of ppy chelate being 3.892 Å and 3.891 Å, respectively.

the ppy ligand is sandwiched between the phenyl groups on each of the two P^O chelates (see dash lines, Figure 2). Their reduced centroid–centroid contacts of 3.891–3.892 Å symbolized the formation of a non-negligible intra-molecular ππ stacking interaction, which is analogous to those reported in the isoelectronic Re^{I} and Os^{II} complexes with two *trans*-substituted phosphine ligands.[19] This interaction is expected to reveal red-shifted singlet ππ* and metal-to-ligand charge transfer (MLCT) bands in the UV/Vis absorption spectra, prolonged lifetime of ^{3}MLCT, and blue-shifted ^{3}MLCT transition versus the congeners without such interaction.[19a] The analogous correlation can not be delineated in the present system owing to the lack of related dialkylphosphino derivatives.

Photophysical Properties

The absorption spectra of **1**–**6** in CH_2Cl_2 solution are depicted in Figure 3. For the pair of ppy complexes **1** and **4**, strong absorption bands in the UV region are reasonably assigned to the ligand-centered ππ* transition involving ppy ligands. Similar to that of **4**, for which its MLCT transition appears at 348 nm, complex **1** exhibits respective MLCT absorption at a slightly lower energy region of 356 nm. Moreover, for

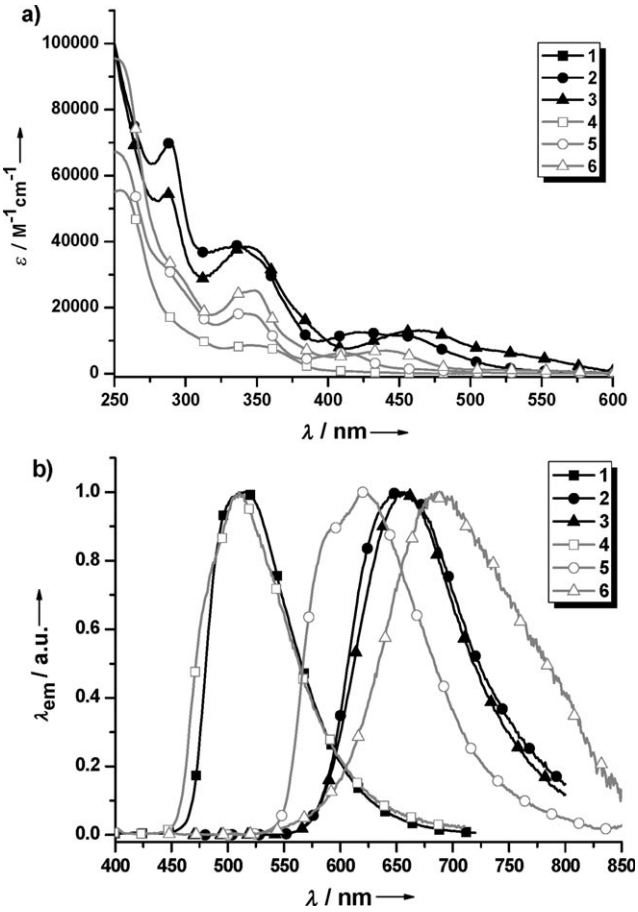

Figure 3. a) Absorption and b) photoluminscence spectra of complex **1**–**6** recorded in CH_2Cl_2 solution at room temperature.

complex **1**, it is reasonable to assign the lowest energy shoulder extending into the visible region to spin-orbit coupling enhanced ^{3}ππ* and ^{3}MLCT transitions, whereas for complex **4**, such absorption to the triplet manifold is obscure. This difference could arise from the possession of a single cyclometalated ligand in **4** and the reduced MLCT contribution (vide infra), such that the corresponding transition probabilities, and hence the absorption extinction coefficients are decreased.

Like their analogues **1** and **4**, the other pairs of piq complexes **2** and **5**, as well as nazo complexes **3** and **6** exhibit the spin allowed ππ* absorption at around 423, 464, 411, and 441 nm, respectively. The lower energy absorption band at 457 and 535 nm for **2** and **3**, are tentatively assigned to the singlet MLCT transition, while the next lower energy absorptions are attributed to the spin-orbit coupling enhanced ^{3}ππ* and ^{3}MLCT transitions. Analogous to the aforementioned differences between **1** and **4**, their counterparts **5** and **6** bearing dual P^O chelates exhibited only the singlet MLCT absorption at 411 and 441 nm, but failed to show the notable ^{3}ππ* and ^{3}MLCT bands arising from the reduced extinction coefficients discussed earlier.

Figure 3 also depicts emission spectra of the titled complexes in CH_2Cl_2, while pertinent photophysical data are listed in Table 1. Moderate to highly intensive luminescence (Φ_p ~ 0.015–0.67, see Table 1) was observed for all complexes in degassed CH_2Cl_2 solution. The entire emission band originating from a triplet state manifold was ascertained by the O_2 quenching rate constant as high as $1.5–2.0\times10^9\,M^{-1}s^{-1}$. For clarity, the data are categorized into two classes, namely series **I** and **II**, anchored by single P^O and dual P^O chelates, respectively. As a result, the emission peak wavelength is in the order of **1** (515 nm) < **2** (652 nm) < **3** (657 nm) for series **I**, and **4** (510 nm) < **5** (620 nm) < **6** (690 nm) for series **II**. Thus, it is obvious that the emission gap as a function of ligand chromophore follows the trend ppy > piq > nazo.[16] Since pyridine (in ppy), isoquinoline (in piq), and quinazoline (in nazo) contribute to the LUMO for both the **I** and **II** series of complexes (vide infra), the results are well rationalized by the decrease of the ππ* energy upon either elongation of π electron conjugation (ppy vs piq) or the additive electron withdrawing nitrogen atom in the fused heterocycle (piq vs nazo).[20] This viewpoint is also supported by the electrochemical data, of which the reduction potential plays a major role to account for the emission gap in both the **I** and **II** series of complexes.

On the other hand, a certain correlation between the **I** and **II** series was also noted in terms of emission energy gap and other photophysical characteristics. Firstly, for the compounds bearing the same ligand chromophore, it is worthwhile to note that the trends of the emission wavelengths follow **2** > **5**, but **3** < **6**. The blue shift observed for **5** versus **2**, from our viewpoint, could arise from the increase of ligand-centered ππ* character at excited states and a concomitant decrease of MLCT contribution (22.02% vs 14.05%, vide infra) as shown in Table 2; the latter tends to possess a much reduced energy gap versus the respective

Table 1. Photophysical and electrochemical properties of Ir^{III} complexes **1–6** in CH_2Cl_2 at room temperature.

	UV/Vis λ_{max} [$\varepsilon\times10^3$, $M^{-1}cm^{-1}$][a]	em λ_{max} [nm]	Φ [%]	τ_{obs} [μs]	k_r	k_{nr}	$E_{1/2}^{ox}$ [ΔE_p][b]/V	$E_{1/2}^{red}$ [ΔE_p][b]/V
1	258 (74), 300 (25), 356 (10), 390 (6.6), 424 (3.6)	515	8.9	0.11	8.3×10^5	8.4×10^6	0.40 (110)	−2.76[d]
2	289 (70), 345 (37), 423 (12), 457 (11)	652	25.0	1.55	1.6×10^5	5.0×10^5	0.41 (140)	−2.27 (130), −2.59 (150)
3	287 (55), 342 (38), 464 (13), 535 (5.8)	657	18.0	0.96	1.8×10^5	8.9×10^5	0.53 (130)	−1.85 (100), −2.16 (130)
4	254 (55), 296 (12), 348 (8.5)	510	1.8	0.05	4.1×10^5	2.2×10^7	0.35[c]	−2.66[d]
5	276 (37), 341 (18), 411 (6.2)	591, 620	67.8	5.09	1.3×10^5	6.3×10^4	0.36[c]	−2.33 (70)
6	294 (31), 348 (25), 441 (7.0), 550 (0.9)	690	1.5	0.10	1.5×10^5	9.8×10^6	0.41[c]	−2.00 (110)

[a] The systematic error of the absorption coefficients measurement is ~±20%. [b] $E_{1/2}$ refers to $[(E_{pa}+E_{pc})/2]$ where E_{pa} and E_{pc} are the anodic and cathodic peak potentials referenced to the Fc^+/Fc couple. $\Delta E_p=|E_{pa}-E_{pc}|$ was reported in mV, and the oxidation and reduction experiments were conducted in CH_2Cl_2 and THF solution, respectively. [c] E_{pa}. [d] E_{pc}.

ππ* transition. In contrast, complexes **3** and **6** show the HOMO principally located on the phenyl group of nazo chelates in **3** and phenolate fragment of P^O ligand in **6**. Since the phenyl group possesses a much lowered energy level compared with that of the phenolate, switching of the HOMO leads to a reduction of emission energy gap and bathochromic shift for **6**. Secondly, based on the same chromophore ligand, that is, ppy, piq, or nazo, the deduced radiative decay rate constant reveals a trend of **I** > **II**, such as **1** > **4**, **2** > **5**, and **3** > **6**. The result is in agreement with the conclusion drawn in the discussion of absorption data, in which the MLCT contribution to the lowest triplet state is reduced in the **II** complexes, resulting in a weaker spin-orbit coupling and hence a smaller radiative decay rate constant for the phosphorescence.[21] In sharp contrast, no apparent correlation was observed for the non-radiative decay rate constant (k_{nr}) and hence the emission quantum yields, which does not seem unreasonable because both chromophore and ancillary ligands vary simultaneously in series **I** and **II**. Nevertheless, as shown in Table 1, the emission quantum yield seems to increase for blue-green (**1** and **4**) to orange-red emission (**2** and **5**) and then decreases in the deep red region (**3** and **6**). The result can be rationalized, in a qualitative manner, by the fact that higher energy emission (e.g., **1**, **4**) is increasingly subject to radiationless channels associated with those high-energy states of shallow potential such as $d_\pi d_{\sigma^*}$ and/or πd_{σ^*} transitions with repulse potential energy surfaces,[22] while deep red emission (e.g., **3** and **6**) is normally quenched by certain high-frequency vibration modes, i.e., the operation of energy gap law.[23]

Table 2. The excitation energies, oscillation strengths, MLCT% of complexes **1–6**.[a]

	States	λ_{cal} [nm]	Assignments	F	MLCT
1	S_1	407.0	HOMO→LUMO(+81%), HOMO-1→LUMO(+12%)	0.0058	13.97%
	T_1	457.2	HOMO-1→LUMO(+41%), HOMO-2→LUMO+1(+21%)		22.02%
2	S_1	485.0	HOMO→LUMO(+87%)	0.0058	13.54%
	T_1	568.9	HOMO-2→LUMO+1(+70%), HOMO-1→LUMO+1(15%)		22.25%
3	S_1	540.9	HOMO→LUMO(+83%), HOMO→LUMO+1(13%)	0.0062	10.53%
	T_1	564.9	HOMO→LUMO(+47%), HOMO-1→LUMO(+14%), HOMO→LUMO+1(14%), HOMO-2→LUMO+1(+13%)		12.25%
4	S_1	434.2	HOMO→LUMO(+96%)	0.0005	11.97%
	T_1	446.4	HOMO-2→LUMO(+55%), HOMO-4→LUMO(+23%), HOMO→LUMO(+10%)		18.02%
5	S_1	520.4	HOMO→LUMO(+97%)	0.0002	7.57%
	T_1	562.6	HOMO-2→LUMO(+54%), HOMO-3→LUMO(+45%)		14.09%
6	S_1	600.5	HOMO→LUMO(+97%)	0.0001	6.05%
	T_1	602.8	HOMO→LUMO(+95%)		13.02%

[a] Some transitions were omitted due to its small contribution (<10%).

To gain more fundamental insight into the above experimental results, we then performed theoretical calculations to investigate the underlying photophysical properties of complexes **1–6**. The results are summarized in Table 2 and Figure 4. Owing to the similarity between **2** and **3** as well as **5** and **6** (vide infra), Figure 4 only depicts the frontier orbitals for **1**, **2**, **4**, and **5**. As revealed in Figure 4 and Table 2, the lowest-energy singlet excited state (S_1) is dominated by the HOMO→LUMO transition for compounds **1–6**. For complex **1**, the HOMO→LUMO transition is mainly ascribed to the metal d_π orbital and the π orbital of the phenolate of the P^O moiety→pyridine in ppy, namely, MLCT and ligand-to-ligand charge transfer (LLCT) transitions, respectively. On the other hand, the same transition of **2** and **3** can be ascribed to an intra-ligand charge transfer (phenyl→isoquinoline or quinazoline in piq or nazo; ILCT) mixed with MLCT. As for the $S_0\rightarrow T_1$ transition of **1–3**, the excitation character is relatively complicated and is composed of more than one type of transition involving, for example, HOMO-1→LUMO and HOMO-2→LUMO (see Table 2). We thus intended not to analyze each transition but simply assigned the first triplet state of **1–3** to a mixing character of ILCT, LLCT, and MLCT.

The HOMO of complexes **4–6** are composed of the d_π orbital of Ir^{III} together with the π orbital of the phenolate ligand. Other occupied orbitals involved in the first triplet state of **4–6**, for example, HOMO-2, reside in the Ir^{III} atom and phenyl moiety of the ppy ligand in **4**, piq ligand in **5**, and nazo ligand in **6**. The LUMO of **4–6** are mainly ascribed to the π* orbital of pyridine in ppy of **4**, isoquinoline in piq of **5**, and quinazoline in nazo of **6**. It is thus reasonable to ascribe the lowest singlet excited state of **4–6** to a LLCT state mixed with MLCT and the triplet excited state of **4–6** to a mixed LLCT and MLCT plus an increased proportion of ILCT character. Moreover, although the %MLCT obtained in this approach is qualitative, the calculated value

CHEMISTRY
AN ASIAN JOURNAL

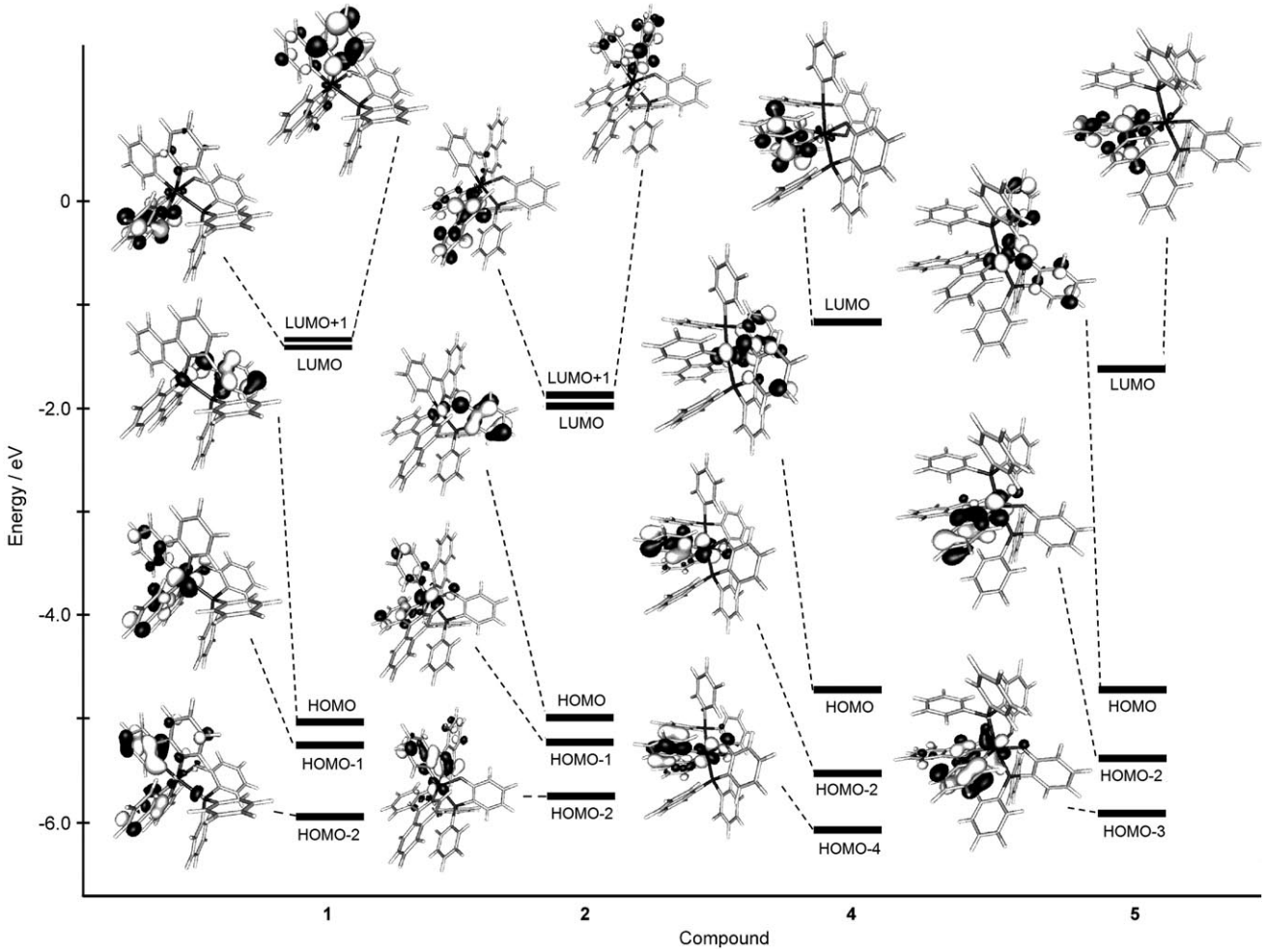

Figure 4. The frontier orbitals of complexes **1**, **2**, **4**, and **5**.

follows the trend of **1** > **4**, **2** > **5**, and **3** > **6** (see Table 2), consistent with the conclusions made from both absorption and emission studies (vide supra).

The calculated energy gap, in terms of wavelength, is blue-shifted from that of the emission data for all complexes studied. We believe that this discrepancy mainly arises from the neglect of the solvent effect or nodeless pseudopotential.[24] Nevertheless, in terms of the S_0-T_1 energy gap, which is revealed by the phosphorescence peak frequency experimentally, the computational results show the trend of **1** > **2** > **3** and **4** > **5** > **6** (see Table 2), consistent with those obtained experimentally (Table 1). In fact, the results also predict that the phosphorescence emission, in terms of peak wavelength, should be in the approximate order of **4** ~ **1** < **5** < **2** < **3** < **6**, again in good agreement with the experimental data. However, we also have to point out that during this approach, only the scalar relativistic effect is taken into account, while the spin-orbit coupling effect on the excitation energies is neglected in almost all TDDFT calculations for heavy elements. The neglect of the spin-orbit coupling parameter may cause appreciable error in estimating the S_1-T_1 gap. The excitation wavelength of the S_1 state of, for example, **6** is calculated to be nearly the same as that of the T_1 state.[25]

Electrochemistry

The electrochemical behavior of these Ir^{III} metal complexes was investigated by cyclic voltammetry using ferrocene as the internal standard. These results are also listed in Table 1. Interestingly, during the anodic scan in CH_2Cl_2, all Ir^{III} metal complexes **1**–**6** exhibited either quasi-reversible or irreversible oxidation in the range of 0.35–0.53 (Figure 5). Complexes **4**–**6** gave lower oxidation signals in the region 0.35–0.41 V with respect to their counterparts **1**–**3**. This could arise from the presence of two P^O chelates in **4**–**6**, for which, in addition to the Ir^{III} metal oxidation, the excessive donation of the electron from the phenolate fragments to the HOMO gave the reduced oxidation potentials. In contrast, the cyclometalated ligands failed to show a notable influence on the oxidation potential of **4**–**6** because they exhibited no essential contribution to the HOMO, which is in

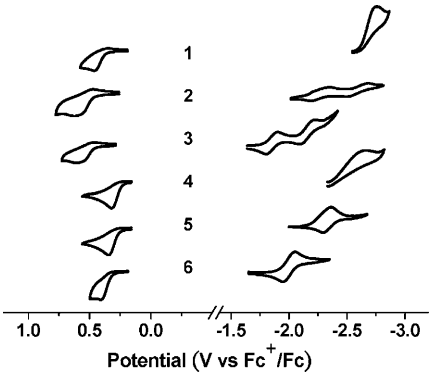

Figure 5. Cyclic voltammograms of all Ir^{III} metal complexes.

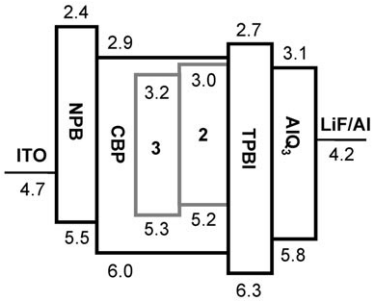

Figure 6. Schematic energy alignment of devices A and B that employed 12 wt.% of **2** and **3** as phosphorescent dopant; energy levels are taken from the following literature citations: NPB and TPBI, CBP, and AlO_3 and LiF/Al.

good agreement with the above theoretical calculation, concluding that the HOMO is mainly ascribed to the phenolate moiety in the P^O chelate.

Upon switching to the cathodic sweep in THF, only one irreversible reduction peak was observed for the ppy complexes **1** and **4**, consistent with the largest energy gap for the ppy ligand as well as the green phosphorescence observed for both of them. On the other hand, two reversible reduction processes, with potentials ranging from −1.85 to −2.59 V, were detected for complexes **2** and **3**, while only one reversible reduction signal was detected at −2.33 and −2.0 V for **5** and **6**, respectively. As revealed in previous studies,[26] the reversible reductions occur primarily on the stronger electron accepting heterocyclic portion of the cyclometalated C^N ligands. Therefore, replacing the piq fragment with a nazo moiety, to afford **3** and **6**, would significantly lower their reduction potentials. This was demonstrated by the observed potentials of **3** (−1.85, −2.16 V) vs those of **2** (−2.27, −2.59 V) and −2.0 V of **6** vs that of −2.33 V of **5**. Moreover, the detection of two reduction peaks in **2** and **3** is attributed to the presence of two cyclometalated ligands within the coordination sphere, thus the second reduction is strongly influenced by the preceding negative charge residing on the first cyclometalated ligand.[27]

OLEDs Characterization

To demonstrate their capabilities in exhibiting decent electroluminescence, we first fabricated red phosphorescence devices based on dopants **2** and **3**, denoted as device A and B, respectively. A multilayer structure of ITO/NPB (40 nm)/CBP:12 wt.% of dopant (30 nm)/TPBI (10 nm)/AlQ_3 (30 nm)/LiF (10 Å)/Al (150 nm) is employed. This device architecture resembles those reported in literature,[28] for which the abbreviations NPB, CBP, TPBI, and AlQ_3 stand for 4,4′-bis[*N*-(1-naphthyl)-*N*-phenylamino] biphenyl, 4,4′-*N*,*N*′-dicarbazolyl-1,1′-bipheny, 1,3,5-tris(*N*-phenyl benzimidizol-2-yl)benzene, and tris(8-hydroxyquinolinato) aluminum (III), and act as hole-transporting, host, hole-blocking, and electron-transporting materials, respectively. Their relative energy alignment is shown in Figure 6,[29] while all crucial performance characteristics are collected in Table 3.

Table 3. Performance data for OLEDs fabricated using complexes **2** and **3** as dopant.

Entry	**A**	**B**
Dopant	**2**	**3**
Max. luminance[a]	46521 (14.0)	57369 (13.5)
E.Q.E. [%][b]	11.8 (8.8)	12.4 (10.1)
Luminance [cd m^{-2}][b]	3472 (12952)	2917 (11791)
L.E. [cd A^{-1}][b]	17.4 (13.0)	14.7 (11.9)
P.E. [lm W^{-1}][b]	6.6 (4.0)	6.8 (4.3)
λ_{max} [(nm)/(CIE_{xy})][c]	618 (0.63, 0.37)	628 (0.65, 0.34)
Turn-on (V)	3.2	3.2

[a] Values in the parentheses are the applied driving voltage. [b] Data recorded at 20 mA cm^{-2}, values in the parentheses are recorded at 100 mA cm^{-2}. [c] Measured at the driving voltage of 8 V.

Both devices exhibited a relatively low turn-on voltage of 3.2 V and decent EL efficiencies. At a current density of 20 mA cm^{-2}, the external quantum efficiency, luminous efficiency, and power efficiency were 12.4%, 14.7 cd A^{-1}, and 6.8 lm W^{-1} for the **3**-based device, respectively, and 11.8%, 17.4 cd A^{-1}, and 6.6 lm W^{-1} for the **2**-based device, respectively. As shown in Figure 7, the **3**-doped device showed a notable bathochromic shift (λ_{max} = 628 nm) compared to that of the device based on dopant **2** with λ_{max} = 618 nm, giving a corresponding Commission Internationale de L′Eclairage ($CIE_{x,y}$) chromaticity coordinates of (0.65, 0.34) and (0.63, 0.37), both are very close to the NTSC red standard (0.66, 0.33). The better red color purity of **3** over **2** is obviously a result of its lowered LUMO energy level resulting from the relatively more stabilized π* orbital of nazo ligands.

Furthermore, our red-emitting devices exhibited a much lower efficiency roll-off at high brightness. Particularly for the **3**-based device, the EL efficiencies remained above 10.1%, 11.9 cd A^{-1}, and 4.3 lm W^{-1} at 100 mA cm^{-2}; while the external quantum efficiency can still be maintained at a level as high as 7.8% upon increasing to 300 mA cm^{-2}, which are quite respectable for the best red-emitting PhOLEDs. Finally, bright luminescence of over 57369 cd m^{-2} and 46521 cd m^{-2} were observed for devices based on **3** and **2** at the driving voltage of 13.5 and 14.0 V, respectively. The better performance can be attributed to a shorter phosphorescence radiative lifetime,[4,30] together with the presence of

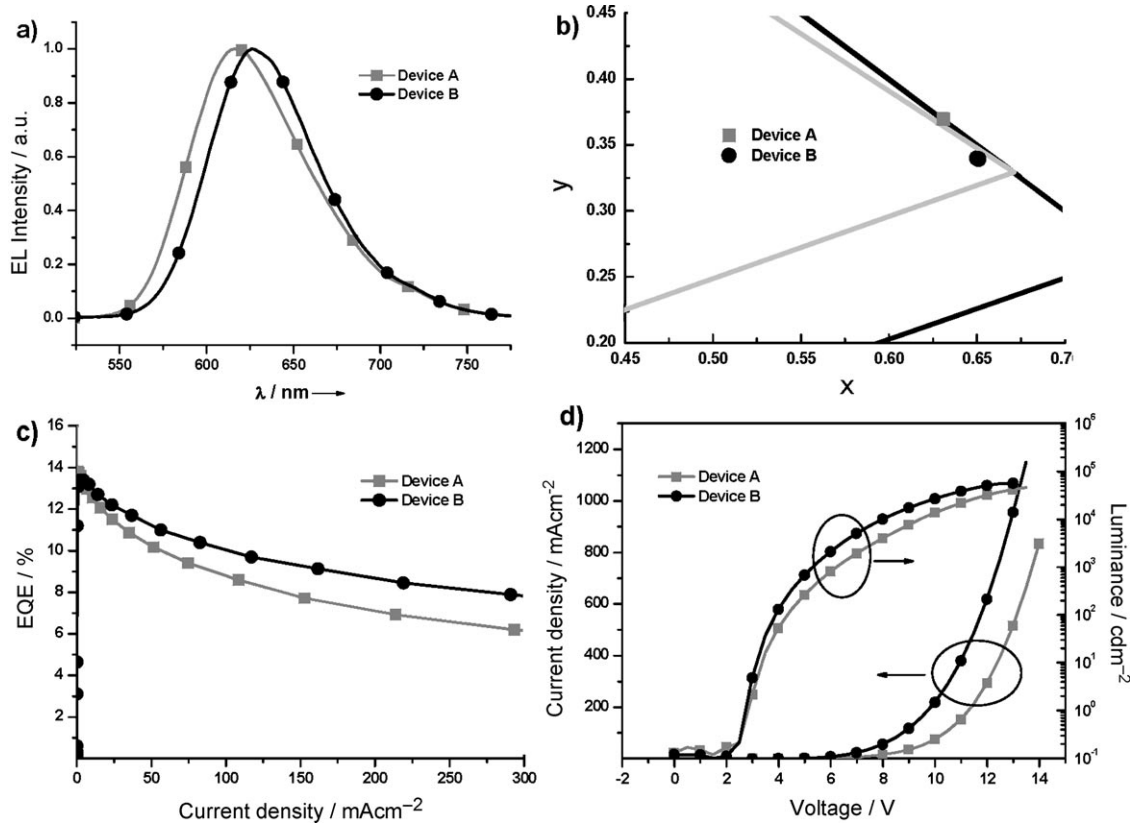

Figure 7. a) EL spectra; b) CIE coordinates; c) external quantum efficiency; d) dependence of current density and luminance versus driving voltage for devices A and B.

unique P^O chelate that may suppress the solid-state aggregation and stabilize the metal complexes using a PPh_2 fragment.

To investigate their potential as dopants suitable for industrial applications, we then tested the lifetime of **3**-based OLEDs with two slightly different architectures. Devices C possessed the layered configuration of ITO/CuPc (7 nm)/NPB (30 nm)/**EL** (25 nm)/AlQ_3 (60 nm)/LiF (0.3 Å)/Al (150 nm), for which CuPc was selected as buffer to adjust the surface smoothness of ITO and provide good adhesion to the NPB charge transport material, while two types of **EL**, namely, CBP+12% **3** and (4,4′-bis(carbazol-9-yl)terphenyl) CTP+12% **3**, were used to evaluate the influence of host materials on the OLED device lifetime. The respective behavior of hole blocking materials was next tested with the series of devices D, which possess the analogous configuration of ITO/CuPc (7 nm)/NPB (30 nm)/CTP+12% **3** (25 nm)/**HBM** (10 nm)/AlQ_3 (60 nm)/LiF (0.3 Å)/Al (150 nm). Note that three hole blocking materials (HBM), namely, 2,9-dimethyl-4,7-diphenyl-1,10-phenanthroline (BCP), TPBI, and aluminum(III) bis(2-methyl-8-quinolinato)(4-phenylphenolate) (BAlq), were alternatively selected for this study.

Allowing the initial luminance to be 500 cd m^{-2}, the lifetime data of all OLED devices C and D were determined by measuring the elapsed time for the luminance to decay to half of its initial value. These estimated lifetime data are summarised in Table 4. It is notable that the device C2 with CTP as host material shows a better lifetime, of over 33000 h, than the device C1 employing CBP as the host material (18000 h). Moreover, the lifetime was also strongly affected by the hole blocking materials (**HBM**), as shown in the series of devices D. Although both TPBI and BCP showed a drastic reduction of lifetime, the lifetime of more than 36000 h was registered by using BAlq, the hole blocking material. The result thus revealed a strong influence imposed by the inherent characteristics of both host and hole blocking materials. Taking these OLED lifetime data into account, together with the fact that the PPh_2 group of P^O chelate is known to be a strong-field ligand, it is reasonable to expect that dopant **3** could render a bright prospect toward commercial application and should attract a broad spectrum of interest in the field of OLEDs.

Table 4. Lifetime data of PhOLEDs doped with 12 wt.% of **3**.

Devices	Host	HBM[a]	lifetime [h]
C1	CBP	–	18334
C2	CTP	–	33053
D1	CTP	TPBI	1197
D2	CTP	BCP	1047
D3	CTP	BAlq	36303

[a] HBM = hole blocking material.

Conclusions

In summary, we report here the design concept as well as preparation of a series of emissive Ir^{III} complexes employing ancillary P^O chelate, for which its PPh_2 fragment is well known for the excellent π-accepting characteristics and classified as a strong-field ligand, while the phenolate segment is more electron donating and capable of facilitating stable metal–ligand bonding. Moreover, the corresponding photophysical properties and DFT calculations suggest that this P^O ligand would only exert a secondary influence, that is, provide a stable and rigid coordination framework, while its participation could fine-tune the light-emitting electronic transition according to the observed photophysical data. Moreover, OLEDs fabricated using 12 wt.% of **3** doped in CBP together with TPBI as hole blocking material gave bright electroluminescence, for which the current and power efficiencies were 14.7 cd $A^{-1}$and 6.8 lm W^{-1} at 20 mA cm^{-2}, and giving the CIE_{xy} chromaticity of 0.65, 0.34 at a driving voltage of 8 V. Finally, one set of the tentatively tested devices employing CuPc as passive layer, CTP + 12 wt.% of **3** as emitting layer, and BAlq as hole blocking material, shows a remarkable lifetime up to 36000 h at an initial luminance of 500 cd m^{-2}. Based on these findings, the aforementioned Ir^{III} metal complexes, particularly nazo derivative **3** can be a promising candidate for real optoelectronic applications, after conducting minor modifications to the molecular structure.

Experimental Section

General Procedures

All reactions were performed under nitrogen. Solvents were distilled from appropriate drying agents prior to use. Commercially available reagents were used without further purification unless otherwise stated. Reactions were monitored by TLC with Merck pre-coated glass plates (0.20 mm with fluorescent indicator UV_{254}). Compounds were visualized with UV light irradiation at 254 nm and 365 nm. Flash column chromatography was carried out using silica gel from Merck (230–400 mesh). Mass spectra were obtained on a JEOL SX-102 A instrument operating in electron impact (EI) mode or fast atom bombardment (FAB) mode. ^1H and ^{13}C NMR spectra were recorded on Varian Mercury-400 or INOVA-500 instruments. The Ir^{III} complexes $[(ppy)_2Ir(\mu\text{-}Cl]_2$, $[(piq)_2Ir(\mu\text{-}Cl]_2$, and $[(nazo)_2Ir(\mu\text{-}Cl]_2$ were obtained from treatment of $IrCl_3{\cdot}3H_2O$ with phenylpyridine (ppyH), 1-phenylisoquinoline (piqH), and 4-phenylquinazoline (nazoH), respectively;[31] while 2-diphenylphosphinophenol (P^OH) was prepared according to the literature methods.[32]

Synthesis and Characterization

Preparation of $[(ppy)_2Ir(P\text{^}O)]$ (1). To a 25 mL flask was added $[(ppy)_2Ir(\mu\text{-}Cl)]_2$ (107 mg, 0.1 mmol), 2-(diphenylphosphino)phenol (P^OH, 61 mg, 0.22 mmol), Na_2CO_3 (106 mg, 1.0 mmol), and 2-methoxyethanol (10 mL). The mixture was heated at 120 °C for 1.5 h, and quenched by addition of deionized water (15 mL) after cooling. The precipitate was filtered and dried under high vacuum. Purification was carried out by silica gel column chromatography eluting with ethyl acetate. Recrystallization from a mixture of CH_2Cl_2 and hexane gave a pale yellow crystalline solid $[(ppy)_2Ir(P\text{^}O)]$ (**1** 80 mg, 0.05 mmol) in 51% yield.

Spectral data for 1. ^1H NMR (400 MHz, $CDCl_3$, 298 K, TMS): $\delta = 8.37$ (d, $J_{H,H} = 5.2$ Hz, 1H), 8.06 (d, $J_{H,H} = 5.6$ Hz, 1H), 7.81–7.74 (m, 3H), 7.59–7.53 (m, 2H), 7.43 (td, $J_{H,H} = 7.8$, 1.6 Hz, 1H), 7.39–7.30 (m, 4H), 7.27 (d, $J_{H,H} = 7.2$ Hz, 1H), 7.24–7.19 (m, 2H), 7.03 (dd, $J_{H,H} = 7.6$, 6.0 Hz, 1H), 6.97 (t, $J_{H,H} = 6.0$ Hz, 1H), 6.88–6.82 (m, 3H), 6.82–6.76 (m, 4H), 6.62 (t, $J_{H,H} = 6.4$ Hz, 2H), 6.53 (t, $J_{H,H} = 8.4$ Hz, 2H), 6.42 (t, $J_{H,H} = 6.0$ Hz, 1H), 6.07 ppm (dd, $J_{H,H} = 6.8$, 4.4 Hz, 1H); $^{31}P\text{-}\{^1H\}$ NMR (202 MHz, $CDCl_3$, 298 K, TMS): $\delta = 12.30$ ppm (s, 1P); MS (FAB, ^{192}Ir): *m*/*z* (%) calcd for $C_{40}H_{30}IrN_2OP$: 777.87 $[M]^+$, 623.68 $[M\text{-ppy}]^+$; found: 778 (100), 624(24); elemental analysis: calcd (%) for $C_{40}H_{30}IrN_2OP$: C 61.76, H 3.89, N 3.60; found: C 61.45, H 4.24, N 3.68.

Preparation of $[(piq)_2Ir(P\text{^}O)]$ (2). Following the procedure described for **1**, a mixture of $[(piq)_2Ir(\mu\text{-}Cl]_2$ (64 mg, 0.05 mmol), P^OH (31 mg, 0.11 mmol), and Na_2CO_3 (53 mg, 0.5 mmol) was refluxed for 1.5 h to provide a red solid (27 mg, 0.03 mmol, 31%).

Spectral data for 2. ^1H NMR (400 MHz, $CDCl_3$, 298 K, TMS): $\delta = 8.88$ (d, $J_{H,H} = 8.0$ Hz, 1H), 8.55 (d, $J_{H,H} = 8.0$ Hz, 1H), 8.37 (d, $J_{H,H} = 6.5$ Hz, 1H), 8.17 (d, $J_{H,H} = 8.5$ Hz, 1H), 8.10 (d, $J_{H,H} = 8.5$ Hz, 1H), 7.99 (d, $J_{H,H} = 6.5$ Hz, 1H), 7.76 (t, $J_{H,H} = 8.3$ Hz, 3H), 7.71–7.66 (m, 3H), 7.59–7.55 (m, 2H), 7.45 (t, $J_{H,H} = 7.3$, 1H), 7.42 (t, $J_{H,H} = 6.8$ Hz, 1H), 7.35 (t, $J_{H,H} = 8.0$ Hz, 2H), 7.20 (t, $J_{H,H} = 7.0$ Hz, 1H), 7.17 (d, $J_{H,H} = 6.5$ Hz, 1H), 7.01 (t, $J_{H,H} = 8.0$ Hz, 1H), 6.97 (t, $J_{H,H} = 8.0$ Hz, 1H), 6.91 (t, $J_{H,H} = 7.0$ Hz, 1H), 6.81 (d, $J_{H,H} = 7.0$ Hz, 1H), 6.80 (d, $J_{H,H} = 7.0$ Hz, 1H), 6.76 (t, $J_{H,H} = 7.8$ Hz, 1H), 6.65 (d, $J_{H,H} = 8.0$ Hz, 1H), 6.60 (t, $J_{H,H} = 7.3$ Hz, 1H), 6.48–6.45 (m, 4H), 6.39–6.37 ppm (m, 2H); $^{31}P\text{-}\{^1H\}$ NMR (202 MHz, $CDCl_3$, 298 K, TMS): $\delta = 13.31$ ppm (s, 1P); MS (FAB, ^{192}Ir): *m*/*z* (%) calcd for $C_{48}H_{34}IrN_2OP$: 877.99 $[M]^+$; found: 878 (100); elemental analysis: calcd (%) for $C_{48}H_{34}IrN_2OP$: C 65.66, H 3.90, N 3.19; found: C 65.33, H 4.12, N 3.06.

Preparation of $[(nazo)_2Ir(P\text{^}O)]$ (3). Following the procedure described for **1**, a mixture of $[(nazo)_2Ir(\mu\text{-}Cl]_2$ (64 mg, 0.05 mmol) and P^OH (31 mg, 0.11 mmol) was refluxed for 2 h to provide a red solid (57 mg, 0.06 mmol, 65%).

Spectral data for 3. ^1H NMR (400 MHz, $CDCl_3$, 298 K, TMS): $\delta = 9.21$ (s, 1H), 8.80 (d, $J_{H,H} = 7.2$ Hz, 1H), 8.65 (s, 1H), 8.44 (d, $J_{H,H} = 8.4$ Hz, 1H), 8.28 (d, $J_{H,H} = 8.4$ Hz, 1H), 8.17 (d, $J_{H,H} = 8.0$ Hz, 1H), 7.93 (t, $J_{H,H} = 7.4$ Hz, 2H), 7.84 (t, $J_{H,H} = 7.6$ Hz, 1H), 7.78–7.68 (m, 4H), 7.59 (t, $J_{H,H} = 7.8$ Hz, 1H), 7.44–7.38 (m, 4H), 7.16 (t, $J_{H,H} = 8.8$ Hz, 1H), 7.03–6.91 (m, 3H), 6.90–6.85 (m, 2H), 6.81 (t, $J_{H,H} = 7.6$ Hz, 1H), 6.60 (t, $J_{H,H} = 7.4$ Hz, 1H), 6.49–6.42 (m, 5H), 6.36 ppm (dd, $J_{H,H} = 8.4$, 4.0 Hz, 1H); $^{31}P\text{-}\{^1H\}$ NMR (202 MHz, $CDCl_3$, 298 K, TMS): $\delta = 12.30$ ppm (s, 1P); MS (FAB, ^{192}Ir): *m*/*z* (%) calcd for $C_{46}H_{32}IrN_4OP$: 879.96 $[M]^+$, 674.73 $[M\text{-nazo}]^+$; found: 880 (40), 675(20); elemental analysis: calcd (%) for $C_{46}H_{32}IrN_4OP$: C 62.79, H 3.67, N 6.37; found: C 62.52, H 3.93, N 6.57.

Preparation of $[(ppy)Ir(P\text{^}O)_2]$ (4). To a 50 mL flask was added $IrCl_3{\cdot}3H_2O$ (100 mg, 0.29 mmol), ppyH (47 mg, 0.3 mmol) and 2-methoxyethanol (35 mL). The mixture was heated at 120 °C for 1.5 h, followed by addition of 2-(diphenylphosphino)phenol (P^OH, 167 mg, 0.6 mmol) and Na_2CO_3 (302 mg, 2.9 mmol), and heating was resumed for another 12 h. After cooling, the mixture was concentrated to 1/3 of its original volume and quenched by addition of deionized water (15 mL), giving yellow precipitate which was collected by filtration. Further purification was carried out by silica-gel column chromatography eluting with a 1:1 mixture of ethyl acetate and hexane. Recrystallization from mixed CH_2Cl_2 and methanol gave yellow crystals $[(ppy)Ir(P\text{^}O)_2]$ (61 mg, 0.07 mmol) in 24% yield.

Spectral data for 4. ^1H NMR (400 MHz, $CDCl_3$, 298 K, TMS): $\delta = 8.50$ (d, $J_{H,H} = 5.3$ Hz, 1H), 8.41–8.37 (m, 2H), 8.21–8.15 (m, 2H), 7.40–7.30 (m, 7H), 7.24–7.00 (m, 7H), 6.95–6.92 (m, 2H), 6.75 (d, $J_{H,H} = 8.0$ Hz, 1H), 6.69–6.57 (m, 8H), 6.47–6.44 (m, 2H), 6.26–6.20 ppm (m, 4H); $^{31}P\text{-}\{^1H\}$ NMR (202 MHz, $CDCl_3$, 298 K, TMS): $\delta = 14.97$ (d, $J_{P,P} = 359$ Hz, 1P), 12.39 ppm (d, $J_{P,P} = 359$ Hz, 1P); MS (FAB, ^{192}Ir): *m*/*z* (%) calcd for $C_{47}H_{36}IrNO_2P_2$: 900.96 $[M]^+$; found: 901 (100); elemental analysis: calcd (%) for $C_{47}H_{36}IrNO_2P_2$: C 62.66, H 4.03, N 1.55; found: C 62.69, H 4.35, N 1.31.

Preparation of $[(piq)Ir(P\text{^}O)_2]$ (5) and $[(nazo)Ir(P\text{^}O)_2]$ (6). Following the procedure described for **4**, treatment of $IrCl_3{\cdot}3H_2O$ and piqH (or nazoH), then with P^OH in a molar ratio of 1:1:2 provides the orange complexes $[(piq)Ir(P\text{^}O)_2]$ (**5**) and $[(nazo)Ir(P\text{^}O)_2]$ (**6**) in 30% and 5% yields, respectively.

Spectral data for 5. ^{1}H NMR (400 MHz, $CDCl_3$, 298 K, TMS): $\delta = 8.46$ (d, $J_{H,H} = 6.4$ Hz 1H), 8.36 (td, $J_{H,H} = 7.6$, 1.6 Hz, 2H), 8.19 (td, $J_{H,H} = 7.0$, 1.6 Hz, 2H), 8.02 (d, $J_{H,H} = 8.8$ Hz, 1H), 7.54 (d, $J_{H,H} = 7.6$ Hz, 1H), 7.47–7.30 (m, 10H), 7.23–7.20 (m, 2H), 7.15~7.00 (m, 4H), 6.93~6.88 (m, 2H), 6.70–6.64 (m, 2H), 6.50–6.39 (m, 7H), 6.22–6.13 ppm (m, 4H); ^{31}P-{^{1}H} NMR (202 MHz, $CDCl_3$, 298 K, TMS): $\delta = 15.32$ (d, $J_{P,P} = 355$ Hz, 1P), 12.79 ppm (d, $J_{P,P} = 355$ Hz, 1P); MS (FAB, ^{192}Ir): m/z (%) calcd for $C_{51}H_{38}IrNO_2P_2$: 951.02 $[M]^+$; found: 951 (100); elemental analysis: calcd (%) for $C_{51}H_{38}IrNO_2P_2$: C 64.41, H 4.03, N 1.47; found: C 64.87, H 4.28, N 1.45.

Spectral data for 6. ^{1}H NMR (400 MHz, $CDCl_3$, 298 K, TMS): $\delta = 9.17$ (s, 1H), 8.42–8.38 (m, 2H), 8.24–8.23 (m, 2H), 7.98 (d, $J_{H,H} = 8.4$ Hz, 1H), 7.77 (dd, $J_{H,H} = 8.0$, 0.8 Hz, 1H), 7.63 (td, $J_{H,H} = 6.6$, 1.2 Hz, 1H), 7.46–7.34 (m, 9H), 7.20–7.12 (m, 5H), 7.06–7.00 (m, 1H), 6.93–6.92 (m, 1H), 6.74–6.71 (m, 2H), 6.51–6.43 (m, 7H), 6.22–6.17 ppm (m, 4H); ^{31}P-{^{1}H} NMR (202 MHz, $CDCl_3$, 298 K, TMS): $\delta = 15.31$ (d, $J_{P,P} = 346$ Hz, 1P), 13.19 ppm (d, $J_{P,P} = 346$ Hz, 1P); MS (FAB, ^{192}Ir): m/z (%) calcd for $C_{50}H_{37}IrN_2O_2P_2$: 952.01 $[M]^+$; found: 952 (100); elemental analysis: calcd (%) for $C_{50}H_{37}IrN_2O_2P_2$: C 63.08, H 3.92, N 2.94; found: C 62.72, H 3.65, N 2.91.

Measurement of Photophysical Data

Steady-state absorption and emission spectra were recorded by a Hitachi (U-3310) spectrophotometer and an Edinburgh (FS920) fluorimeter, respectively. Both the wavelength-dependent excitation and emission response of the fluorimeter were calibrated. A configuration of front-face excitation was used to measure the emission of the solid sample, in which the cell was made by assembling two edge-polished quartz plates with various Teflon spacers. A combination of appropriate filters was used to avoid the interference from the scattering light. Lifetime studies were performed by an Edinburgh FL 900 photon-counting system with a hydrogen-filled/or a nitrogen lamp as the excitation source. Data were analyzed using the nonlinear least squares procedure in combination with an iterative convolution method. The emission decays were analyzed by the sum of exponential functions, which allows partial removal of the instrument time broadening and consequently renders a temporal resolution of ~200 ps.

Electrochemical Measurement

Cyclic voltammetry (CV) measurements were performed using a BAS 100 B/W electrochemical analyzer. The oxidation and reduction measurements were recorded using Pt wire and a Au disk coated with Hg as working electrodes, respectively. Experiments were performed in anhydrous CH_2Cl_2 and anhydrous THF containing 0.1 M (TBA)PF_6 as the supporting electrolyte, at a scan rate of 50 mV s^{-1}. The potentials were measured against a Ag/AgCl (0.01 M $AgNO_3$) reference electrode with ferrocene as the internal standard.

X-ray Structural Analysis

Single crystal X-ray diffraction data of complexes **3** and **4** were measured on a Bruker Smart CCD diffractometer using $\lambda(Mo_{K\alpha})$ radiation ($\lambda = 0.71073$ Å). The data collection was executed using the SMART program. Cell refinement and data reduction were made with the SAINT program. The structure was determined using the SHELXTL/PC program and refined using full-matrix least squares. All non-hydrogen atoms were refined anisotropically, whereas hydrogen atoms were placed at the calculated positions and included in the final stage of refinements with fixed parameters. The respective crystallographic refinement parameters are summarized in Table 5.

CCDC 717863 and CCDC 717864 contain the supplementary crystallographic data for this paper. These data can be obtained free of charge from The Cambridge Crystallographic Data Centre at www.ccdc.cam.ac.uk/data_request/cif.

Computational Methodology

Time-dependent PBE0 calculations are based on the geometry optimized structures at the PBE0 level. The basis set for the geometry optimization and the excitation energy calculation are both a double-ζ quality basis set consisting of Hay and Wadt's quasi-relativistic effective core potentials (LANL2DZ) for an Ir^{III} atom;[33] a 6-31G* basis set was employed for the H, C, N, O, and P atoms. Typically, the lowest triplet and singlet roots of the nonhermitian eigenvalue equations were obtained to determine the vertical excitation energies. Oscillator strengths were deduced from the dipole transition matrix elements (for singlet states only). All the calculations were performed with the Gaussian 03 package.[34]

Fabrication of Light-Emitting Devices

The EL devices were fabricated by vacuum deposition of the materials at 10^{-6} torr onto a clean glass that was pre-coated with a layer of indium tin oxide with a sheet resistance of 25 Ω/□. Various organic layers were deposited sequentially at a rate of 1–2 Å s^{-1}. Phosphorescent dopant was co-evaporated along with CBP by two independent source reservoirs. A thin layer of LiF (1 nm) and a thick layer of Al (150 nm) were sequentially deposited at the cathode. The active area of the emitting diode was 9.00 mm^2. The current-voltage-luminance of the devices was measured in ambient conditions with a Keithley 2400 Source meter and a Newport 1835C Optical meter equipped with an 818ST silicon photodiode. The EL spectrum was obtained using a Hitachi F4500 spectrofluorimeter.

Lifetime Measurements

All devices for lifetime measurements were prepared by thermal evaporation in a high vacuum system with a pressure better then 5×10^{-4} Pa without breaking the vacuum. ITO-coated glass plates with a surface resistivity ≤ 15 Ω/□ were used as substrate. They were ultrasonically

Table 5. Crystal data and structure refinement parameters for complexes **3** and **4**.

complex	**3**·2×$CHCl_3$·1/2×C_6H_{14}	**4**·THF
Empirical formula	$C_{51}H_{41}Cl_6IrN_4OP$	$C_{51}H_{44}IrNO_3P_2$
Formula mass [g mol^{-1}]	1161.75	973.01
T [K]	150(2) K	150(2) K
Crystal system	triclinic	monoclinic
Space group	$P\bar{1}$	$P2_1/c$
a [Å]	9.6916(5)	9.3059(6)
b [Å]	12.7650(6)	27.004(2)
c [Å]	20.348(1)	16.545(1)
α [°]	102.604(1)°	90°
β [°]	100.826(1)°	98.440(1)°
γ [°]	102.647(1)°	90°
Volume, Z	2322.5(2) Å^3, 2	4112.7(5) Å^3, 4
ρ_{calcd} [Mg m^{-3}]	1.661	1.571
μ [mm^{-1}]	3.298	3.370
F(000)	1154	1952
Crystal dimensions [mm]	0.40×0.17×0.17	0.25×0.12×0.05
Reflections collected	29994	26613
Independent reflections	10631 [R(int) = 0.0382]	9422 [R(int) = 0.0481]
Max. and min. transmission	0.6040 and 0.3521	0.7293 and 0.4862
Data/restraints/parameters	10631/0/578	9422/11/518
Goodness-of-fit on F^2	1.059	1.019
Final R indices [I ≥ 2 σ(I)]	$R^1 = 0.0311$, $wR^2 = 0.0686$	$R^1 = 0.0334$, $wR^2 = 0.0704$
R indices (all data)	$R^1 = 0.0349$, $wR^2 = 0.0701$	$R^1 = 0.0475$, $wR^2 = 0.0763$
Largest diff. peak and hole	0.982 and −0.838 e Å^{-3}	1.083 and −0.774 e Å^{-3}

cleaned at first and then treated by oxygen plasma for work function tuning. During the evaporation process the deposition rates were monitored by several controllers, which were calibrated by a Dektak 6M surface profiler from Veeco. These devices were encapsulated with an UV curing adhesive in a nitrogen atmosphere before lifetime testing. The OLED lifetime test system Polaronix M6000 from Mac Science was used for lifetime measurement in an accelerated mode constant current mode at room temperature.

Acknowledgements

This work was funded by the National Science Council of Taiwan, R.O.C. under grants: NSC 93-2113M-007-012 and NSC 93-2752M-002-002-PAE. We are also grateful to the National Center for High-performance Computing for computer time and facilities.

[1] a) P.-T. Chou, Y. Chi, *Eur. J. Inorg. Chem.* **2006**, 3319; b) F. Babudri, G. M. Farinola, F. Naso, R. Ragni, *Chem. Commun.* **2007**, 1003; c) L. Flamigni, A. Barbieri, C. Sabatini, B. Ventura, F. Barigelletti, *Top. Curr. Chem.* **2007**, *281*, 143; d) M. K. Nazeeruddin, M. Grätzel, *Struct. Bonding* **2007**, *123*, 113; e) F. So, J. Kido, P. Burrows, *MRS Bull.* **2008**, *33*, 663; f) J. A. G. Williams, A. J. Wilkinson, V. L. Whittle, *Dalton Trans.* **2008**, 2081.

[2] a) K. Dedeian, J. Shi, N. Shepherd, E. Forsythe, D. C. Morton, *Inorg. Chem.* **2005**, *44*, 4445; b) S. Chew, C. S. Lee, S.-T. Lee, P. Wang, J. He, W. Li, J. Pan, X. Zhang, H. Kwong, *Appl. Phys. Lett.* **2006**, *88*, 093510.

[3] a) C. Adachi, M. A. Baldo, S. R. Forrest, M. E. Thompson, *Appl. Phys. Lett.* **2000**, *77*, 904; b) G. He, O. Schneider, D. Qin, X. Zhou, M. Pfeiffer, K. Leo, *J. Appl. Phys.* **2004**, *95*, 5773; c) D. Yang, W. Li, B. Chu, D. Zhang, J. Zhu, Z. Su, W Su, L. Han, D. Bi, Y. Chen, F. Yan, H. Liu, D. Wang, *Appl. Phys. Lett.* **2008**, *92*, 253309.

[4] S. Okada, K. Okinaka, H. Iwawaki, M. Furugori, M. Hashimoto, T. Mukaide, J. Kamatani, S. Igawa, A. Tsuboyama, T. Takiguchi, K. Ueno, *Dalton Trans.* **2005**, 1583.

[5] a) J. Li, P. I. Djurovich, B. D. Alleyne, M. Yousufuddin, N. N. Ho, J. C. Thomas, J. C. Peters, R. Bau, M. E. Thompson, *Inorg. Chem.* **2005**, *44*, 1713; b) C.-J. Chang, C.-H. Yang, K. Chen, Y. Chi, C.-F. Shu, M.-L. Ho, Y.-S. Yeh, P.-T. Chou, *Dalton Trans.* **2007**, 1881; c) P.-I. Shih, C.-H. Chien, C.-Y. Chuang, C.-F. Shu, C.-H. Yang, J.-H. Chen, Y. Chi, *J. Mater. Chem.* **2007**, *17*, 1692; d) Y.-M. Wang, F. Teng, L.-H. Gan, H.-M. Liu, X.-H. Zhang, W.-F. Fu, Y.-S. Wang, X.-R. Xu, *J. Phys. Chem. C* **2008**, *112*, 4743.

[6] a) W.-Y. Wong, G.-J. Zhou, X.-M. Yu, H.-S. Kwok, B.-Z. Tang, *Adv. Funct. Mater.* **2006**, *16*, 838; b) T. Tsuzuki, S. Tokito, *Adv. Mater.* **2007**, *19*, 276; c) X. Wei, J. Peng, J. Cheng, M. Xie, Z. Lu, C. Li, Y. Cao, *Adv. Funct. Mater.* **2007**, *17*, 3319; d) G. Zhou, C.-L. Ho, W.-Y. Wong, Q. Wang, D. Ma, L. Wang, Z. Lin, T. B. Marder, A. Beeby, *Adv. Funct. Mater.* **2008**, *18*, 499.

[7] Y. You, H. S. Huh, K. S. Kim, S. W. Lee, D. Kim, S. Y. Park, *Chem. Commun.* **2008**, 3998.

[8] a) Y. You, K. S. Kim, T. K. Ahn, D. Kim, S. Y. Park, *J. Phys. Chem. C* **2007**, *111*, 4052; b) Y. You, S. H. Kim, H. K. Jung, S. Y. Park, *Macromolecules* **2006**, *39*, 349; c) Y. Byun, W. S. Jeon, T.-W. Lee, Y.-Y. Lyu, S. Chang, O. Kwon, E. Han, H. Kim, M. Kim, H.-J. Lee, R. R. Das, *Dalton Trans.* **2008**, 4732.

[9] L. Chen, H. You, C. Yang, D. Ma, J. Qin, *Chem. Commun.* **2007**, 1352.

[10] a) S.-J. Yeh, M.-F. Wu, C.-T. Chen, Y.-H. Song, Y. Chi, M.-H. Ho, S.-F. Hsu, C. H. Chen, *Adv. Mater.* **2005**, *17*, 285; b) L.-L. Wu, C.-H. Yang, I.-W. Sun, S.-Y. Chu, P.-C. Kao, H.-H. Huang, *Organometallics* **2007**, *26*, 2017; c) S.-Y. Chang, J.-L. Chen, Y. Chi, Y.-M. Cheng, G.-H. Lee, C.-M. Jiang, P.-T. Chou, *Inorg. Chem.* **2007**, *46*, 11202; d) Y.-M. Cheng, G.-H. Lee, P.-T. Chou, L.-S. Chen, Y. Chi, C.-H. Yang, Y.-H. Song, S.-Y. Chang, P.-I. Shih, C.-F. Shu, *Adv. Funct. Mater.* **2008**, *18*, 183; e) C.-F. Chang, Y.-M. Cheng, Y. Chi, Y.-C. Chiu, C.-C. Lin, G.-H. Lee, P.-T. Chou, C.-C. Chen, C.-H. Chang, C.-C. Wu, *Angew. Chem.* **2008**, *120*, 4618; *Angew. Chem. Int. Ed.* **2008**, *47*, 4542; f) E. Orselli, R. Q. Albuquerque, P. M. Fransen, R. Froehlich, H. M. Janssen, L. De Cola, *J. Mater. Chem.* **2008**, *18*, 4579; g) S. Stagni, S. Colella, A. Palazzi, G. Valenti, S. Zacchini, F. Paolucci, M. Marcaccio, R. Q. Albuquerque, L. De Cola, *Inorg. Chem.* **2008**, *47*, 10509.

[11] S. Lamansky, P. Djurovich, D. Murphy, F. Abdel-Razzaq, R. Kwong, I. Tsyba, M. Bortz, B. Mui, R. Bau, M. E. Thompson, *Inorg. Chem.* **2001**, *40*, 1704.

[12] a) S.-Y. Chang, J. Kavitha, S.-W. Li, C.-S. Hsu, Y. Chi, Y.-S. Yeh, P.-T. Chou, G.-H. Lee, A. J. Carty, Y.-T. Tao, C.-H. Chien, *Inorg. Chem.* **2006**, *45*, 137; b) I. Avilov, P. Minoofar, J. Cornil, L. De Cola, *J. Am. Chem. Soc.* **2007**, *129*, 8247.

[13] A. van Dijken, A. Perro, E. A. Meulenkamp, K. Brunner, *Org. Electron.* **2003**, *4*, 131.

[14] Y.-C. Chiu, J.-Y. Hung, Y. Chi, C.-C. Chen, C.-H. Chang, C.-C. Wu, Y.-M. Cheng, Y.-C. Yu, G.-H. Lee, P.-T. Chou, *Adv. Mater.* **2009**, DOI:adma.200802546.

[15] C.-H. Yang, Y.-M. Cheng, Y. Chi, C.-J. Hsu, F.-C. Fang, K.-T. Wong, P.-T. Chou, C.-H. Chang, M.-H. Tsai, C.-C. Wu, *Angew. Chem.* **2007**, *119*, 2470; *Angew. Chem. Int. Ed.* **2007**, *46*, 2418.

[16] F.-M. Hwang, H.-Y. Chen, P.-S. Chen, C.-S. Liu, Y. Chi, C.-F. Shu, F.-I. Wu, P.-T. Chou, S.-M. Peng, G.-H. Lee, *Inorg. Chem.* **2005**, *44*, 1344.

[17] a) A. Tsuboyama, H. Iwawaki, M. Furugori, T. Mukaide, J. Kamatani, S. Igawa, T. Moriyama, S. Miura, T. Takiguchi, S. Okada, M. Hoshino, K. Ueno, *J. Am. Chem. Soc.* **2003**, *125*, 12971; b) S.-Y. Chang, Y.-M. Cheng, Y. Chi, Y.-C. Lin, C.-M. Jiang, G.-H. Lee, P.-T. Chou, *Dalton Trans.* **2008**, 6901.

[18] a) C. S. Chin, M.-S. Eum, S. Y. Kim, C. Kim, S. K. Kang, *Eur. J. Inorg. Chem.* **2006**, 4979; b) M.-S. Eum, C. S. Chin, S. Y. Kim, C. Kim, S. K. Kang, N. H. Hur, J. H. Seo, G. Y. Kim, Y. K. Kim, *Inorg. Chem.* **2008**, *47*, 6289.

[19] a) H. Tsubaki, A. Sekine, Y. Ohashi, K. Koike, H. Takeda, O. Ishitani, *J. Am. Chem. Soc.* **2005**, *127*, 15544; b) Y.-L. Tung, P.-C. Wu, C.-S. Liu, Y. Chi, J.-K. Yu, Y.-H. Hu, P.-T. Chou, S.-M. Peng, G.-H. Lee, Y. Tao, A. J. Carty, C.-F. Shu, F.-I. Wu, *Organometallics* **2004**, *23*, 3745.

[20] H.-Y. Chen, Y. Chi, C.-S. Liu, J.-K. Yu, Y.-M. Cheng, K.-S. Chen, P.-T. Chou, S.-M. Peng, G.-H. Lee, A. J. Carty, S.-J. Yeh, C.-T. Chen, *Adv. Funct. Mater.* **2005**, *15*, 567.

[21] Y.-M. Cheng, E. Y. Li, G.-H. Lee, P.-T. Chou, S.-Y. Lin, C.-F. Shu, K.-C. Hwang, Y.-L. Chen, Y.-H. Song, Y. Chi, *Inorg. Chem.* **2007**, *46*, 10276.

[22] a) J.-K. Yu, Y.-H. Hu, Y.-M. Cheng, P.-T. Chou, S.-M. Peng, G.-H. Lee, A. J. Carty, Y.-L. Tung, S.-W. Lee, Y. Chi, C.-S. Liu, *Chem. Eur. J.* **2004**, *10*, 6255; b) Y. Chi, P.-T. Chou, *Chem. Soc. Rev.* **2007**, *36*, 1421.

[23] a) E. M. Kober, J. V. Caspar, R. S. Lumpkin, T. J. Meyer, *J. Phys. Chem.* **1986**, *90*, 3722; b) J. A. Treadway, B. Loeb, R. Lopez, P. A. Anderson, F. R. Keene, T. J. Meyer, *Inorg. Chem.* **1996**, *35*, 2242.

[24] a) A. V. Titov, N. S. Mosyagin, V. F. Ezhov, *Phys. Rev. Lett.* **1996**, *77*, 5346; b) W. C. Ermler, M. M. Marino, *J. Chem. Inf. Comput. Sci.* **2001**, *41*, 77; c) A. V. Titov, N. S. Mosyagin, *Int. Photogr. Int. J. Quant. Chem.* **1999**, *71*, 359; d) A. V. Titov, *Int. J. Quantum Chem.* **1998**, *57*, 453.

[25] a) J. Gao, W. Liu, B. Song, C. Liu, *J. Chem. Phys.* **2004**, *121*, 6658; b) D. Toffoli, M. Stener, P. Decleva, *Phys. Rev. A* **2002**, *66*, 012501; c) D. Toffoli, M. Stener, and P. Decleva, *J. Phys. B* **2002**, *35*, 1275; d) D. Toffoli, M. Stener, P. Decleva, *J. Phys. B* **2003**, *36*, 3097; e) F. Wang, T. Ziegler, E. van Lenthe, S. van Gisbergen, E. J. Baerends, *J. Chem. Phys.* **2005**, *122*, 204103.

[26] a) Y. Ohsawa, S. Sprouse, K. A. King, M. K. DeArmond, K. W. Hanck, R. J. Watts, *J. Phys. Chem.* **1987**, *91*, 1047; b) J. Brooks, Y. Babayan, S. Lamansky, P. I. Djurovich, I. Tsyba, R. Bau, M. E. Thompson, *Inorg. Chem.* **2002**, *41*, 3055; c) A. B. Tamayo, B. D. Alleyne, P. I. Djurovich, S. Lamansky, I. Tsyba, N. N. Ho, R. Bau, M. E. Thompson, *J. Am. Chem. Soc.* **2003**, *125*, 7377.

[27] a) I.-S. Shin, J. I. Kim, T.-H. Kwon, J.-I. Hong, J.-K. Lee, H. Kim, *J. Phys. Chem. C* **2007**, *111*, 2280; b) A. Kapturkiewicza, J. Nowackib, P. Borowicza, *Electrochimica Acta* **2005**, *50*, 3395.

[28] a) B. W. D'Andrade, M. E. Thompson, S. R. Forrest, *Adv. Mater.* **2002**, *14*, 147; b) Y.-L. Tung, L.-S. Chen, Y. Chi, P.-T. Chou, Y.-M. Cheng, E. Y. Li, G.-H. Lee, C.-F. Shu, F.-I. Wu, A. J. Carty, *Adv. Funct. Mater.* **2006**, *16*, 1615; c) J.-W. Kang, S.-H. Lee, H.-D. Park, W.-I. Jeong, K.-M. Yoo, Y.-S. Park, J.-J. Kim, *Appl. Phys. Lett.* **2007**, *90*, 223508; d) C.-H. Chien, S.-F. Liao, C.-H. Wu, C.-F. Shu, S.-Y. Chang, Y. Chi, P.-T. Chou, C.-H. Lai, *Adv. Funct. Mater.* **2008**, *18*, 1430.

[29] a) Y.-S. Park, J.-W. Kang, D. M. Kang, J.-W. Park, Y.-H. Kim, S.-K. Kwon, J.-J. Kim, *Adv. Mater.* **2008**, *20*, 1957; b) Z. Q. Gao, B. X. Mi, H. L. Tam, K. W. Cheah, C. H. Chen, M. S. Wong, S. T. Lee, C. S. Lee, *Adv. Mater.* **2008**, *20*, 774; c) Y.-Y. Lyu, J. Kwak, O. Kwon, S.-H. Lee, D. Kim, C. Lee, K. Char, *Adv. Mater.* **2008**, *20*, 2720.

[30] a) Y.-L. Tung, S.-W. Lee, Y. Chi, Y.-T. Tao, C.-H. Chien, Y.-M. Cheng, P.-T. Chou, S.-M. Peng, C.-S. Liu, *J. Mater. Chem.* **2005**, *15*, 460; b) C.-L. Ho, W.-Y. Wong, Z.-Q. Gao, C.-H. Chen, K.-W. Cheah, B. Yao, Z. Xie, Q. Wang, D. Ma, L. Wang, X.-M. Yu, H.-S. Kwok, Z. Lin, *Adv. Funct. Mater.* **2008**, *18*, 319.

[31] Y.-H. Song, S.-J. Yeh, C.-T. Chen, Y. Chi, C.-S. Liu, J.-K. Yu, Y.-H. Hu, P.-T. Chou, S.-M. Peng, G.-H. Lee, *Adv. Funct. Mater.* **2004**, *14*, 1221.

[32] a) J. Heinicke, M. Koehler, N. Peulecke, M. He, M. K. Kindermann, W. Keim, G. Fink, *Chem. Eur. J.* **2003**, *9*, 6093; b) E. Marzi, J. Gorecka, M. Schlosser, *Synthesis* **2004**, *10*, 1609.

[33] a) P. J. Hay, W. R. Wadt, *J. Chem. Phys.* **1985**, *82*, 270; b) W. R. Wadt, P. J. Hay, *J. Chem. Phys.* **1985**, *82*, 284; c) P. J. Hay, W. R. Wadt, *J. Chem. Phys.* **1985**, *82*, 299.

[34] *Gaussian 03*, Revision C.02, M. J. Frisch, G. W. Trucks, H. B. Schlegel, G. E. Scuseria, M. A. Robb, J. R. Cheeseman, J. A. Montgomery, Jr., T. Vreven, K. N. Kudin, J. C. Burant, J. M. Millam, S. S. Iyengar, J. Tomasi, V. Barone, B. Mennucci, M. Cossi, G. Scalmani, N. Rega, G. A. Petersson, H. Nakatsuji, M. Hada, M. Ehara, K. Toyota, R. Fukuda, J. Hasegawa, M. Ishida, T. Nakajima, Y. Honda, O. Kitao, H. Nakai, M. Klene, X. Li, J. E. Knox, H. P. Hratchian, J. B. Cross, V. Bakken, C. Adamo, J. Jaramillo, R. Gomperts, R. E. Stratmann, O. Yazyev, A. J. Austin, R. Cammi, C. Pomelli, J. W. Ochterski, P. Y. Ayala, K. Morokuma, G. A. Voth, P. Salvador, J. J. Dannenberg, V. G. Zakrzewski, S. Dapprich, A. D. Daniels, M. C. Strain, O. Farkas, D. K. Malick, A. D. Rabuck, K. Raghavachari, J. B. Foresman, J. V. Ortiz, Q. Cui, A. G. Baboul, S. Clifford, J. Cioslowski, B. B. Stefanov, G. Liu, A. Liashenko, P. Piskorz, I. Komaromi, R. L. Martin, D. J. Fox, T. Keith, M. A. Al-Laham, C. Y. Peng, A. Nanayakkara, M. Challacombe, P. M. W. Gill, B. Johnson, W. Chen, M. W. Wong, C. Gonzalez, J. A. Pople, Gaussian, Inc., Wallingford CT, **2004**.

Received: December 15, 2008
Revised: January 29, 2009
Published online: March 17, 2009

